Staphylococcus aureus binds to the N-terminal region of corneodesmosin to adhere to the stratum corneum in atopic dermatitis

Aisling M. Towell[a], Cécile Feuillie[b], Pauline Vitry[b], Thaina M. Da Costa[a], Marion Mathelié-Guinlet[b], Sanja Kezic[c], Orla M. Fleury[a], Maeve A. McAleer[d], Yves F. Dufrêne[b,e], Alan D. Irvine[d], and Joan A. Geoghegan[a,f,1]

[a]Department of Microbiology, Moyne Institute of Preventive Medicine, School of Genetics and Microbiology, Trinity College Dublin, Dublin 2, Ireland; [b]Louvain Institute of Biomolecular Science and Technology, Université Catholique de Louvain, B-1348 Louvain-la-Neuve, Belgium; [c]Coronel Institute of Occupational Health, Amsterdam Public Health Research Institute, University Medical Center, University of Amsterdam, 1105 AZ Amsterdam, The Netherlands; [d]Clinical Medicine, Trinity College Dublin, Dublin 2, Ireland; [e]Walloon Excellence in Life Sciences and Biotechnology, B-1300 Wavre, Belgium; and [f]Institute of Microbiology and Infection, College of Medical and Dental Sciences, University of Birmingham, B15 2TT Birmingham, United Kingdom

Edited by Richard P. Novick, New York University School of Medicine, New York, NY, and approved November 24, 2020 (received for review July 9, 2020)

Staphylococcus aureus **colonizes the skin of the majority of patients with atopic dermatitis (AD), and its presence increases disease severity. Adhesion of *S. aureus* to corneocytes in the stratum corneum is a key initial event in colonization, but the bacterial and host factors contributing to this process have not been defined. Here, we show that *S. aureus* interacts with the host protein corneodesmosin. Corneodesmosin is aberrantly displayed on the tips of villus-like projections that occur on the surface of AD corneocytes as a result of low levels of skin humectants known as natural moisturizing factor (NMF). An *S. aureus* mutant deficient in fibronectin binding protein B (FnBPB) and clumping factor B (ClfB) did not bind to corneodesmosin in vitro. Using surface plasmon resonance, we found that FnBPB and ClfB proteins bound with similar affinities. The *S. aureus* binding site was localized to the N-terminal glycine–serine-rich region of corneodesmosin. Atomic force microscopy showed that the N-terminal region was present on corneocytes containing low levels of NMF and that blocking it with an antibody inhibited binding of individual *S. aureus* cells to corneocytes. Finally, we found that *S. aureus* mutants deficient in FnBPB or ClfB have a reduced ability to adhere to low-NMF corneocytes from patients. In summary, we show that FnBPB and ClfB interact with the accessible N-terminal region of corneodesmosin on AD corneocytes, allowing *S. aureus* to take advantage of the aberrant display of corneodesmosin that accompanies low NMF in AD. This interaction facilitates the characteristic strong binding of *S. aureus* to AD corneocytes.**

colonization | *Staphylococcus aureus* | adhesion | corneocytes | bacteria

Atopic dermatitis (AD) is a chronic inflammatory skin disorder, affecting 15 to 20% of children (1, 2). During disease flares, patients experience painful inflamed skin lesions accompanied by intense itch. Epidermal barrier dysfunction, increased type 2 immune responses, and recurrent skin infections are features of AD (3). The most common cause of infection is *Staphylococcus aureus*. This bacterium colonizes the skin of the majority of AD patients (4, 5). Isolates representing several *S. aureus* lineages are recovered from AD skin; however, strains from the clonal complex 1 (CC1) lineage are the most frequently isolated (6–9). The burden of *S. aureus* on lesional and nonlesional skin correlates with severity of the disease (10, 11). *S. aureus* directly influences pathogenesis, and several factors produced by the bacterium increase inflammation and exacerbate AD symptoms, including staphylococcal superantigen B and delta-toxin (12–15).

Despite the clear association between *S. aureus* colonization and AD disease severity (11), the bacterial and host factor determinants underlying colonization are poorly understood (16). Adhesion is a critical early step in the colonization process. *S. aureus* adheres to corneocytes in the stratum corneum of AD skin (6, 17, 18). We previously found that clumping factor B (ClfB), a cell wall-anchored protein displayed on the surface of *S. aureus*, can mediate adhesion to corneocytes from AD patients (6). ClfB also binds to the alpha chain of fibrinogen and to the cornified envelope proteins loricrin and cytokeratin 10 (K10) in desquamated nasal epithelial cells (19–21). To date, ClfB is the only bacterial factor known to promote adherence to corneocytes in AD. However, a ClfB-deficient mutant retained the ability to bind to corneocytes (6), suggesting that additional bacterial factors are at play.

Filaggrin deficiency is common in patients with established AD and is either genetic or caused by down-regulation of gene expression by Th-2–type cytokines (22–24). Filaggrin deficiency causes epidermal barrier defects and a loss of the hygroscopic filaggrin breakdown products that normally contribute to the natural moisturizing factor (NMF) in corneocytes (25). NMF comprises a collection of humectants, including filaggrin breakdown products urocanic acid and pyrrolidone acid, along with urea, citrate, lactate acid, and sugars, and is responsible for regulating hydration in the skin (26). Low-NMF levels are

Significance

Staphylococcus aureus **colonizes skin of patients with atopic dermatitis (AD), increasing disease severity. Colonization involves bacterial adhesion to skin corneocytes, and elucidating the molecular basis of interactions governing adhesion is crucial to further our understanding of pathogenesis and inform targeted therapies. We identify host and pathogen factors that enable adhesion. We demonstrate that *S. aureus* interacts with the N-terminal region of corneodesmosin on the surface of patient corneocytes. This interaction is mediated by two bacterial cell wall-anchored proteins (fibronectin binding protein B and clumping factor B). Frequency and force of bacterial binding to AD corneocytes decreased when the N-terminal region of corneodesmosin was blocked with an antibody, indicating the contribution of this interaction during *S. aureus* adhesion to human skin.**

Author contributions: A.M.T., C.F., P.V., T.M.D.C., M.M.-G., S.K., Y.F.D., A.D.I., and J.A.G. designed research; A.M.T., C.F., P.V., T.M.D.C., S.K., O.M.F., and M.A.M. performed research; A.M.T., C.F., P.V., T.M.D.C., M.M.-G., S.K., O.M.F., M.A.M., Y.F.D., A.D.I., and J.A.G. analyzed data; and A.M.T., C.F., M.M.-G., S.K., Y.F.D., A.D.I., and J.A.G. wrote the paper.

The authors declare no competing interest.

This article is a PNAS Direct Submission.

[1]To whom correspondence may be addressed. Email: j.geoghegan@bham.ac.uk.

This article contains supporting information online at https://www.pnas.org/lookup/suppl/doi:10.1073/pnas.2014444118/-/DCSupplemental.

Published December 23, 2020.

associated with a loss of hydration, increased disease severity, and abnormal corneocyte morphology (27). We showed recently that *S. aureus* binds more strongly to low-NMF AD corneocytes than to corneocytes with normal levels of NMF (18).

Corneocytes with low NMF have very different surface topography when compared with corneocytes with normal levels of NMF (27). Aberrant "villus-like" projections (VPs) protrude from the surface of low-NMF corneocytes (18, 27). The protein corneodesmosin (CDSN) is confined to the cell–cell junctions between corneocytes in healthy skin, where homophilic interactions between the CDSN proteins on adjacent cells facilitate cell–cell cohesion (28). In AD patients, however, CDSN decorates the tips of the VPs on low-NMF corneocytes (27).

This study aimed to elucidate a key component of *S. aureus* colonization by identifying the molecular determinants of adherence to AD corneocytes. We recognized that the occurrence of VPs on low-NMF corneocytes presents a different colonization surface to the bacterium and postulated that the accessibility of CDSN on the tips of VPs could influence pathogen adherence. We show that *S. aureus* can interact with CDSN and identify the *S. aureus* proteins promoting adherence to this host protein. We use single-cell and single-molecule atomic force microscopy (AFM), surface plasmon resonance (SPR), and ex vivo bacterial adherence studies with patient corneocytes to characterize this interaction. This study expands the repertoire of ligands for *S. aureus* and, crucially, links bacterial interactions with a host protein (CDSN) to binding to corneocytes taken from patients. Thus, our findings provide insights into the adhesion process and develop our understanding of the mechanisms underlying colonization of the skin of AD patients by *S. aureus*.

Results

S. aureus Adheres to CDSN. *S. aureus* binds more avidly to low-NMF corneocytes than to high-NMF corneocytes (18). Given that CDSN is displayed on the tips of the VPs that are abundant on low-NMF corneocytes but appears only on the periphery of high-NMF corneocytes (27), we investigated if CDSN supports adhesion of *S. aureus*. Previous attempts to purify recombinant corneodesmosin (rCDSN) from an *Escherichia coli* expression system were not successful as truncated protein fragments were copurified with the full-length protein during affinity chromatography (28). Here, rCDSN was purified using a two-step purification process, where DNA encoding a Strep tag II affinity tag was linked to the 3′ end of the *CDSN* gene sequence in the vector pGEX-4T2. The resulting protein was purified by Strep-Tactin affinity chromatography followed by glutathione affinity chromatography, which allowed for the selective purification of full-length protein with an N-terminal glutathione S-transferase (GST) tag and a C-terminal Strep tag II (rCDSN) (*SI Appendix*, Fig. S1). To investigate if *S. aureus* could adhere to CDSN, Newman, a laboratory strain used here as a control, and AD08, a representative CC1 strain isolated from the infected skin lesion of a pediatric patient with AD (6), were tested for adherence to rCDSN. Both strains adhered to rCDSN in a dose-dependent manner (Fig. 1 *A* and *B*).

Considering that the *S. aureus* cell wall-anchored protein ClfB promotes adherence of AD08 to low-NMF corneocytes sampled from pediatric AD patients (6), we wondered whether ClfB could mediate adherence of *S. aureus* to CDSN. To study this, isogenic mutants of Newman and AD08 deficient in ClfB were used. Newman *clfB* did not adhere to rCDSN, indicating that adherence of the control strain Newman is completely dependent on ClfB (Fig. 1*A*). AD08Δ*clfB*, however, adhered to rCDSN indistinguishably from the wild type (Fig. 1*B*), suggesting that at least one other *S. aureus* adhesin promotes AD08 adherence to CDSN.

ClfB and Fibronectin Binding Protein B Mediate Adherence of _S. aureus_ to CDSN. Next, we set out to identify factors promoting adherence of clinical isolate AD08 to CDSN. ClfB is part of the microbial surface components recognizing matrix molecules (MSCRAMM) family of adhesins that are covalently linked to the *S. aureus* cell wall (29). The ligand binding activity of MSCRAMMs usually lies in the N2 and N3 subdomains of the protein (29). Fibronectin binding proteins A and B (FnBPA and FnBPB, respectively) are MSCRAMMs that share 39 and 40% amino acid similarity with ClfB, in the N2N3 subdomains. These proteins were of interest to us since both genes (*fnbA* and *fnbB*) contain premature stop codons in strain Newman resulting in the production of truncated proteins that are released by the bacterium, rather than being anchored to the cell wall (30). Thus, Newman does not adhere to fibronectin (30). This prompted us to examine if either of these proteins might facilitate the adherence of *S. aureus* AD08 to CDSN and explain why the AD08Δ*clfB* mutant retains ability to adhere.

AD08 mutants with single- or double-gene deletions in the *clfB*, *fnbA*, and *fnbB* genes were generated. The mutants and wild-type AD08 were grown to exponential phase, and their ability to adhere to immobilized rCDSN was examined. There was no reduction in adherence of AD08Δ*clfB* or AD08Δ*fnbA* to CDSN compared with wild-type AD08; however, there was a significant reduction in adherence by AD08Δ*fnbB* (Fig. 1*C*), indicating that FnBPB contributes to the ability of AD08 to adhere to CDSN. The AD08Δ*fnbA*Δ*fnbB* mutant adhered to CDSN similarly to the single *fnbB* mutant. The adhesion of AD08Δ*clfB*Δ*fnbA* was reduced compared with the wild type at the highest ligand concentrations tested, despite neither single mutation affecting adherence. However, adherence of AD08Δ*clfB*Δ*fnbB* to CDSN was completely abolished (Fig. 1*C*), suggesting that FnBPA alone is insufficient to mediate adherence to CDSN. Complementation of AD08Δ*clfB*Δ*fnbB* with plasmids carrying *clfB* or *fnbB* restored ability to adhere to CDSN (Fig. 1*D*). AD08Δ*clfB*Δ*fnbB* adhered to fibronectin, showing us that FnBPA is produced by this mutant (*SI Appendix*, Fig. S2). Together, these data indicate that FnBPB and ClfB facilitate adherence of *S. aureus* to CDSN, while FnBPA cannot support adherence. Thus, ClfB and FnBPB are CDSN binding proteins.

Recombinant N2N3 Subdomains of ClfB and FnBPB Bind to CDSN. ClfB N2N3 subdomains and FnBPB N2N3 subdomains, with the sequence of the AD08 proteins, were purified from *E. coli*. We examined if the proteins bound to CDSN using SPR. His-tagged CDSN was immobilized, and increasing concentrations of $rClfB_{CC1}N2N3$ or $rFnBPB_{CC1}N2N3$ were passed over the surface. Both proteins bound CDSN in a concentration-dependent manner (Fig. 2). The relative affinity of each interaction was calculated by plotting the binding measured at equilibrium (response units) against concentration of recombinant protein. This provided evidence that ClfB and FnBPB can bind directly to CDSN and that the affinity of each protein for the ligand is similar ($4.46 \pm 2.29 \times 10^{-5}$ M and $4.91 \pm 2.36 \times 10^{-5}$ M, respectively). Furthermore, this finding suggests that the N2N3 subdomains are sufficient to bind to CDSN.

The N-Terminal Glycine–Serine-Rich Loop of CDSN Comprises the _S. aureus_ Binding Site. CDSN contains two glycine- and serine-rich regions, one at the N terminus and one at the C terminus of the mature protein (31) that are predicted to form flexible secondary structures called glycine–serine loops. ClfB binds to glycine–serine-rich loops in K10, loricrin, and fibrinogen (19–21). Therefore, we sought to determine if the glycine–serine-rich regions in CDSN contain the *S. aureus* binding site. GST-tagged variant truncates of rCDSN lacking either the N-terminal loop (ΔNT) or the C-terminal loop (ΔCT) were purified from *E. coli*. AD08 adhered to full-length rCDSN and to rCDSNΔCT but not to ΔNT or recombinant GST (Fig. 3*A*), implying that the C-terminal glycine–serine-rich region

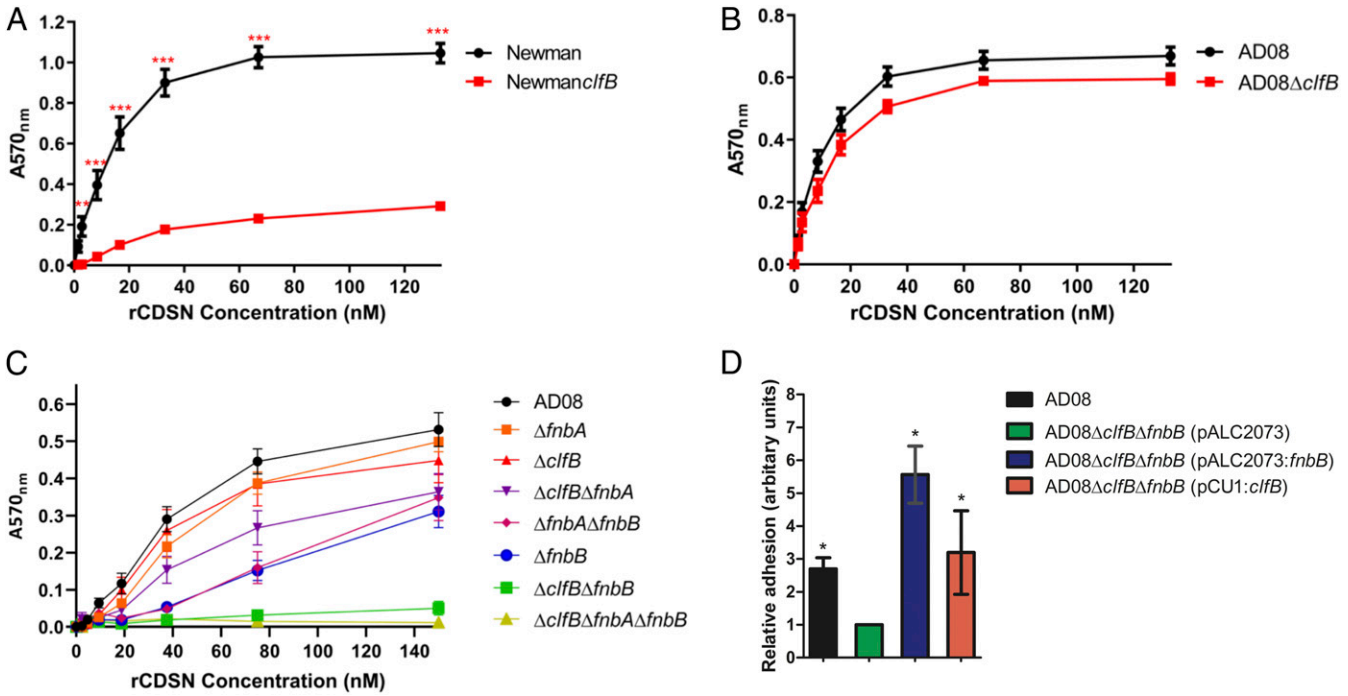

Fig. 1. ClfB and FnBPB mediate adherence of *S. aureus* to CDSN. *S. aureus* was grown to exponential phase (optical density at 600 nm = 0.35) and added to wells of a microtiter plate coated with doubling dilutions (*A*–*C*) or a single concentration (*D*; 80 nM) of rCDSN. Adherent cells were stained using crystal violet, and absorbance was measured at 570 nm (A_{570}). (*A*–*C*) Each datum point represents the mean values of three independent experiments, and error bars show the SEM of the biological replicates. Statistical significance was determined using two-way ANOVA with a Bonferroni posttest to compare variances between the wild type and mutants. (*A* and *B*) No symbol indicates $P > 0.05$. $^{**}P = 0.009$; $^{***}P < 0.001$. (*C*) All mutants except Δ*fnbA* and Δ*clfB* were significantly different to wild-type AD08 at rCDSN concentrations between 37.5 and 150 nM ($P < 0.001$). All mutants except Δ*fnbA*, Δ*clfB*, and Δ*clfB*Δ*fnbA* were significantly different to wild-type AD08 at 18.75 nM rCDSN ($P < 0.05$). There were no significant differences between the wild type and mutants at any other ligand concentrations ($P > 0.05$). (*D*) Statistical significance was determined using one-way ANOVA with a Dunnett posttest to compare variances between AD08Δ*clfB*Δ*fnbB* (pALC2073) and each of the other strains. $^{*}P < 0.05$.

does not support the adherence of *S. aureus* to CDSN; rather, the binding site incorporates the N-terminal region. Mutants expressing a single CDSN binding protein (AD08Δ*clfB*Δ*fnbA* and AD08Δ*fnbA*Δ*fnbB*) exhibited an identical profile of binding to rCDSNΔNT and rCDSNΔCT as the wild type (Fig. 3*B*), indicating that both FnBPB and ClfB recognize the same region of CDSN. The mutant devoid of CDSN binding proteins (AD08Δ*clfB*Δ*fnbB*) did not adhere to rCDSNΔNT or rCDSNΔCT, again demonstrating that FnBPA does not contribute to CDSN adherence. Having established that the C-terminal region was not required to support *S. aureus* adhesion and that the N-terminal region was essential, GST-tagged CDSN N-terminal

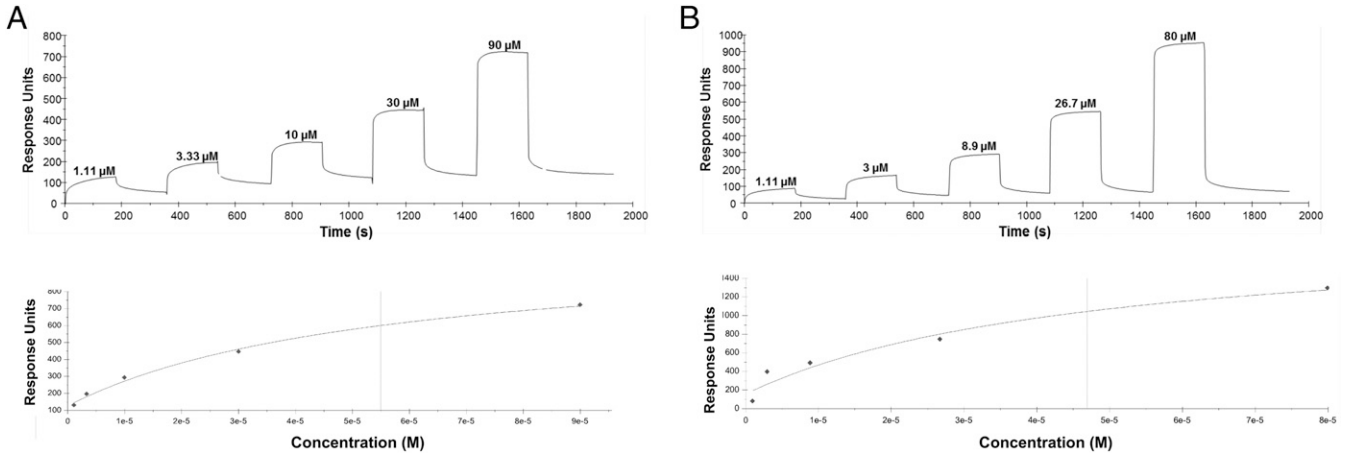

Fig. 2. Recombinant N2N3 subdomains of ClfB and FnBPB bind to CDSN. Representative sensorgrams showing the binding of $rClfB_{CC1}N2N3$ (*A*) and $rFnBPB_{CC1}N2N3$ (*B*) to His-CDSN. His-CDSN was immobilized onto a CM5 chip by amine coupling, and recombinant proteins were passed over the surface at the concentrations indicated. Binding was plotted as response units against time (*Upper*). The sensorgrams shown are representative of those from five individual experiments. The affinities were calculated from curve fitting to a plot of the response unit values against the concentrations of $rClfB_{CC1}N2N3$ or $rFnBPB_{CC1}N2N3$ (*Lower*).

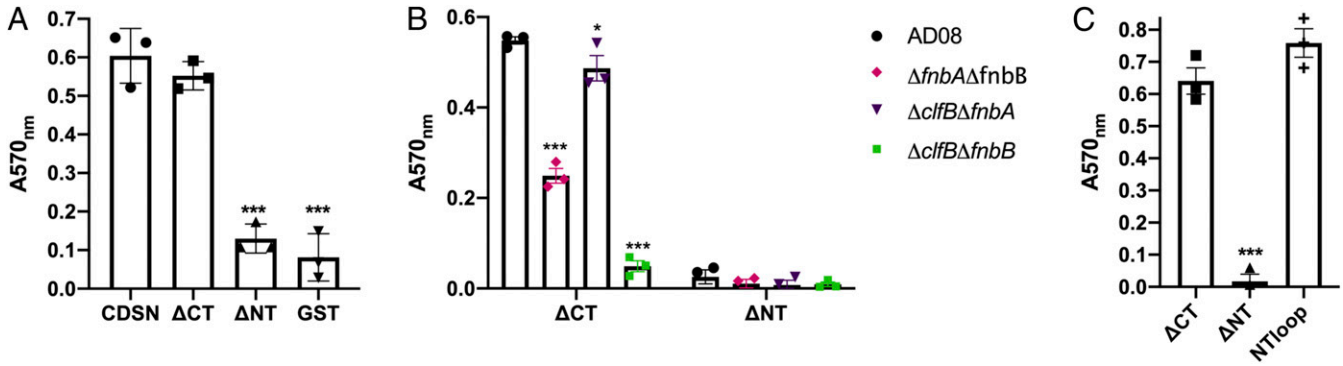

Fig. 3. The N-terminal glycine–serine-rich region of CDSN comprises the *S. aureus* binding site. Bacteria were grown to exponential phase (OD_{600} = 0.35) and added to wells of a microtiter plate coated with (*A*) rCDSN, CDSNΔCT(ΔCT), CDSNΔNT (ΔNT), or GST (66 nM); (*B*) CDSNΔCT or ΔNT (66 nM); and (*C*) recombinant ΔCT, ΔNT, and GST-tagged CDSN N-terminal region (NTloop) (70 nM). Adherent cells were stained with crystal violet, and absorbance was measured at 570 nm (A_{570}). Each symbol represents the data from individual experiments, bars represent the mean of three independent experiments, and error bars show the SEM of the biological replicates. Significance was determined by two two-way ANOVAs using a Dunnett posttest to compare differences to variances between CDSN (circle) and CDSNΔCT (square), CDSNΔNT (up triangle) or GST (down triangle) (*A*) or CDSNΔCT (square) and CDSNΔNT (up triangle) or NTloop (+) (*C*) or one-way ANOVA with Bonferroni posttest to compare variances between AD08 (circle), AD08Δ*fnbAfnbB* (diamond), AD08Δ*clfBfnbA* (down triangle), and AD08Δ*clfBfnbB* (square) (*B*). No symbol indicates $P > 0.05$. * $P < 0.05$, ***$P < 0.001$.

region (NTloop) was purified to establish whether this region alone could support adherence of *S. aureus*. AD08 adhered to CDSN N-terminal region and rCDSNΔCT similarly (Fig. 3*C*). These data indicate that the N-terminal region of CDSN comprises the *S. aureus* binding site.

The N-Terminal Region of CDSN Is Exposed on Low-NMF Corneocytes. Discovering that *S. aureus* adheres to the N-terminal region prompted us to investigate if this part of the CDSN protein is accessible to the bacterium in the human stratum corneum. Specifically, we investigated if the N-terminal region of CDSN is exposed on the surface of low-NMF corneocytes sampled from pediatric patients with AD using an antibody. To do so, we performed single-molecule AFM experiments, which allowed us to probe specific interactions between the antibody and its cognate antigen. We verified the specificity of the antibody for CDSN by demonstrating that it did not cross-react with the other glycine–serine-rich cornified envelope proteins loricrin and K10 (*SI Appendix*, Fig. S3). Functionalizing the AFM tip with this polyclonal immunoglobulin G (IgG), raised against the N-terminal region of the CDSN protein, we were able to associate adhesive events on corneocytes with the presence of the N-terminal region of CDSN, thus locating the protein at the molecular level. Fig. 4 shows the results from force measurements between anti-CDSN tips and corneocytes from a patient with low-NMF levels and, as a control, a subject with high-NMF levels (for each subject, the results from six independent bacterium–corneocyte pairs are pooled). Interestingly, the binding of antibody to the N-terminal region of CDSN occurred more frequently on low-NMF corneocytes than on high-NMF corneocytes (Fig. 4), with binding probabilities of 6.7 ± 2.3% (mean ± SD) and 2.2 ± 0.9% (mean ± SD), respectively. The probability of interaction of anti-CDSN IgG with low-NMF corneocytes was significantly higher than with high-NMF corneocytes, suggesting that the N-terminal region of CDSN is more abundant, or more accessible, on low-NMF corneocytes. Crucially, this indicated that the *S. aureus* binding site within CDSN, as identified in vitro, is available to bacteria on the surface of low-NMF corneocytes in AD patients.

Blocking the N-Terminal Region of CDSN with an Antibody Inhibits Binding of *S. aureus* to Corneocytes from Low-NMF Skin. To determine if binding of *S. aureus* to the N-terminal region of CDSN contributes to the ability of the bacterium to adhere to corneocytes, we examined if antibody raised against the N-terminal region of CDSN was capable of blocking the adhesion of *S. aureus*. We performed single-cell force spectroscopy, where a single living bacterium was immobilized on the AFM probe. This cell probe was used to directly measure the interaction probability and force between the bacterium and tape strips of corneocytes with low NMF. Anti-CDSN antibody fragment [$F(ab')_2$] was added to the experimental medium in increasing concentration (0 to 5 μg/mL), and the binding probability between AD08 bacteria and the corneocyte was measured for four independent cell pairs. This allowed us to directly quantify the blocking effect of the addition of the antibody at the scale of the single bacterium–corneocyte

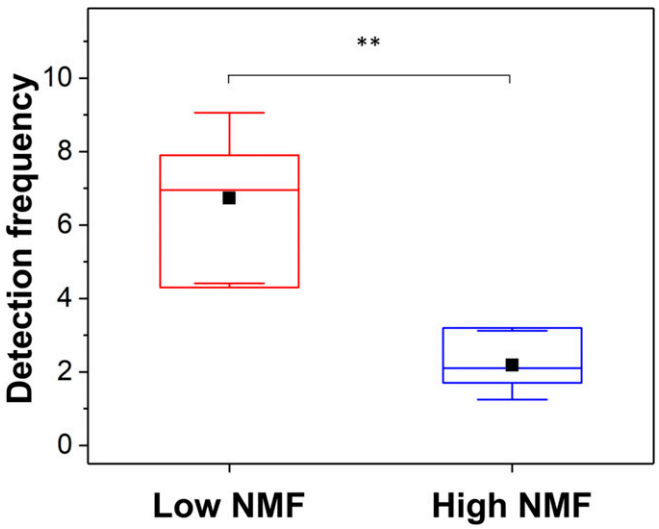

Fig. 4. The N-terminal region of CDSN is exposed on low-NMF corneocytes. Corneocytes were isolated from AD patients with low-NMF levels (patient #1,508) and high-NMF levels (patient #1,493). Single-molecule force spectroscopy was used to measure binding of anti-CDSN IgG immobilized on the AFM tip to the low-NMF corneocytes (red) and high-NMF corneocytes (blue). Box plot shows mean detection frequency (full squares), median, first and third quartiles (boxes), and range of data without outliers (whiskers), and it shows the result of six independent AFM tip/corneocyte replicates in total. Statistical significance was determined using a two-sample Student's *t* test. **$P < 0.01$.

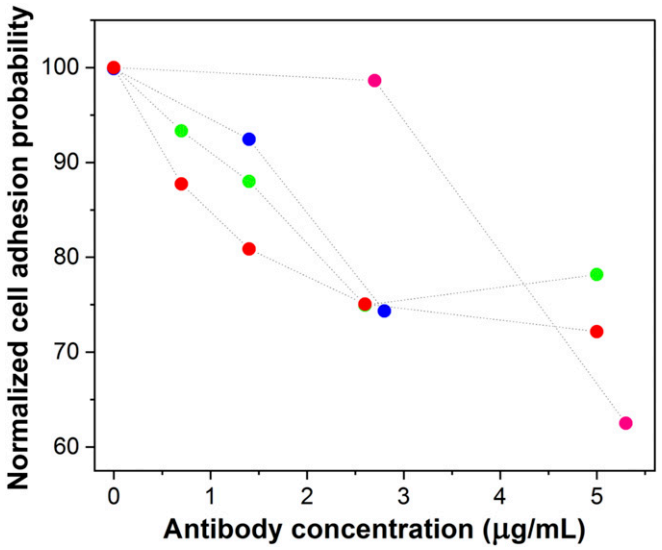

Fig. 5. Blocking the N-terminal region of CDSN with an antibody inhibits binding of *S. aureus* to corneocytes from low-NMF skin. Corneocytes were isolated from an AD patient with low NMF (patient #1,508) and incubated with increasing concentrations of anti-CDSN $F(ab')_2$ fragments. A single cell of wild-type AD08 was immobilized onto an AFM probe. The adhesion probability of the AD08 cell to the corneocyte was measured by single-cell force spectroscopy. All values presented are percentages of the initial adhesion value measured when no $F(ab')_2$ was added. Each color represents an independent experiment where a different bacterium–corneocyte pairing was tested.

pair. The addition of the antibody fragment did interfere with the bacterial cell–corneocyte interaction, and there was a dose-dependent reduction in probability of adhesion for each bacterium–corneocyte pair tested (Fig. 5), suggesting that the ability of AD08 to adhere to AD corneocytes is reduced when the *S. aureus* binding site in CDSN is blocked. We observed variability between cell pairs, with two distinct behaviors: 1) for 3 out of 4 cells, we observed a progressive decrease of the interaction probability with ~25% decrease reached at a concentration of 2.5 μg/mL of $F(ab')_2$ fragment; 2) for one cell, although the binding probability first stayed stable in the lower range of $F(ab')_2$ concentration (0 to 3 μg/mL), it decreased by ~37% upon addition of 4 to 5 μg/mL antibody. Control experiments showed that the anti-CDSN $F(ab')_2$ did not react with the surface of *S. aureus* AD08, indicating that the inhibition was specific and due to blocking of the ligand on corneocytes (*SI Appendix*, Fig. S4). In summary, our analyses show that anti-CDSN [$F(ab')_2$] is a competitive inhibitor of the AD08–corneocyte interaction, which suggests that *S. aureus* targets the N-terminal region of CDSN to adhere to low-NMF corneocytes from AD skin.

ClfB and FnBPB Promote Adherence of *S. aureus* to AD Corneocytes. Having demonstrated the importance of CDSN as a ligand for *S. aureus* on AD corneocytes and a role for ClfB and FnBPB in mediating adherence to CDSN in vitro, the role of these proteins in the adherence of *S. aureus* to the stratum corneum of AD skin was investigated. AD08 and its isogenic ClfB-deficient and FnBPB-deficient mutants were inoculated onto sections of tape strips isolated from low-NMF AD patients to examine if either protein was important for the adherence of *S. aureus* to low-NMF corneocytes. The adherence of AD08Δ*clfB* and AD08Δ*fnbB* was significantly reduced, indicating that each protein contributes to corneocyte adhesion (Fig. 6). A double mutant (AD08Δ*clfB*Δ*fnbB*) had significantly reduced adherence compared with the wild type but not compared with either of the single mutants. These data suggest that both ClfB and FnBPB contribute significantly to corneocyte adhesion.

Discussion

The ability of *S. aureus* to colonize the stratum corneum is strongly associated with disease severity in AD. Yet, the bacterial and host determinants of colonization have not yet been fully elucidated. Here, we identify CDSN as a ligand for *S. aureus* and provide a comprehensive analysis of the interaction between the bacterium and its binding partner. We identify cell wall-anchored proteins FnBPB and ClfB as the factors promoting binding to CDSN and study the *S. aureus* interaction with CDSN using purified proteins, corneocytes coming from AD patients, and bacteria displaying cell wall-anchored proteins. We show that the *S. aureus* binding site is located at the N terminus of CDSN. We then use single-cell AFM to demonstrate that blocking the N terminus of CDSN reduces the interaction of *S. aureus* with the corneocyte surface using an ex vivo adhesion model with corneocytes from AD patients. Finally, we show that an *S. aureus* mutant unable to bind to CDSN has a reduced ability to interact with low-NMF corneocytes. These findings provide insights into bacterial adhesion to the stratum corneum of AD skin. Our analyses use a clinical *S. aureus* isolate from AD and patient corneocytes, thus increasing the clinical relevance and translational potential of this work.

CDSN is aberrantly located on low-NMF corneocytes where it is displayed on the tips of VPs (27, 32). Having established that *S. aureus* targets the N-terminal region of CDSN, we sought to determine if this part of the protein is intact on the surface of low-NMF corneocytes using an antibody raised against the N terminus. This was important because the N-terminal region of CDSN is removed by the proteolytic activity of kallikrein-related peptidase 7 to facilitate desquamation. However, secretion of kallikrein-related peptidase 7 from lamellar granules is impaired in AD, and the serine protease inhibitor Kazal-type 5 is upregulated, resulting in reduced cleavage of CDSN in AD skin (33). In line with this, using single-molecule AFM, we found that the N-terminal region of CDSN was more abundant, and therefore accessible, for binding on low-NMF corneocytes than on high-NMF corneocytes. This finding assured us that the *S. aureus*

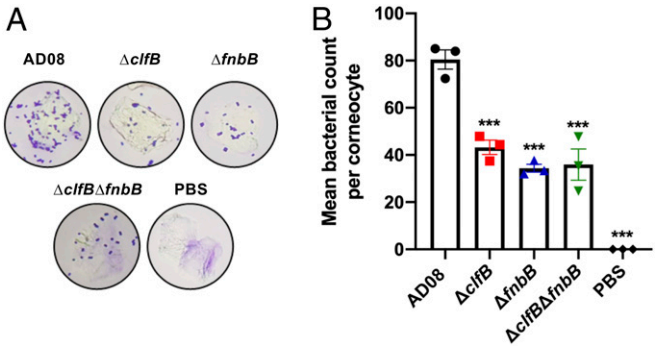

Fig. 6. ClfB and FnBPB promote adherence of *S. aureus* to AD corneocytes. *S. aureus* was grown to exponential phase (OD_{600} = 0.35), and bacteria were incubated with low-NMF AD corneocytes (patients #1,602, #1,654, #1,669). Adherent bacterial cells were stained with crystal violet. (*A*) Representative image of a single corneocyte with adherent bacteria viewed under a light microscope. (*B*) The number of bacteria adhering to 15 corneocytes was counted, and the mean number of wild-type AD08 (circle), AD08Δ*clfB* (square), AD08Δ*fnbB* (up triangle), and AD08Δ*clfB*Δ*fnbB* (down triangle) adhering to a corneocyte is presented. Each datum point is from a different biological replicate, and the bars represent the means of three independent experiments, with error bars showing the SEM. Statistical significance was determined by ANOVA and Dunnett posttest. Where no symbols appear, the differences were not significant ($P > 0.05$). ***$P < 0.001$.

receptor we identified in vitro was available as a ligand for *S. aureus* on the surface of low-NMF corneocytes from AD skin.

MSCRAMMs are displayed on the surface of *S. aureus* and mediate interactions with host molecules and cells. We have discovered that FnBPB and ClfB are CDSN binding proteins. In addition to CDSN, the N2N3 subdomains of FnBPB bind to fibrinogen, elastin, plasminogen, and histone H3 (34–36), while ClfB N2N3 binds to fibrinogen, loricrin, and K10 (19). MSCRAMMs generally bind to ligands using the "dock, lock, and latch" mechanism (29). The presence of glycine–serine-rich sequences within the *S. aureus* binding site in CDSN is in common with other ClfB ligands known to bind by the dock, lock, and latch mechanism (19, 20, 37). We speculate that ClfB binds to all four of its ligands via the same dock, lock, and latch mechanism. However, FnBPB is capable of binding to at least one host factor (plasminogen) by an alternative mechanism (35), and a detailed investigation of the mode of CDSN binding by both MSCRAMMs is needed to provide a deeper understanding of the interaction.

The MSCRAMMs FnBPA and FnBPB share a common domain organization and 48% amino acid identity in their N2N3 subdomains. Despite this, we found that FnBPA does not mediate bacterial adherence to CDSN. The *fnbA* and *fnbB* genes lie adjacent to each other on the chromosome, and a gene duplication event is believed to have given rise to the second gene. It is clear that divergence of these genes has allowed *S. aureus* to expand the diversity of ligands it interacts with. FnBPB binds to CDSN and histone H3, ligands not shared by FnBPA. The sequence of the FnBPB and ClfB N2N3 subdomains varies among *S. aureus* genomes, and higher variation occurs between lineages than within them (38, 39). It is possible that sequence variation can alter the affinity of FnBPB or ClfB for CDSN, and further investigation of variation in protein sequence may shed more light on the precise molecular details of the CDSN–MSCRAMM interaction.

Loricrin and K10 are present in the cornified envelope and cytoskeleton, respectively, of the human stratum corneum (40, 41). Several studies suggest that the genes encoding loricrin and K10 are down-regulated in AD skin (42–44). Knocking down filaggrin expression in a three-dimensional human skin equivalent model increased CDSN protein levels while loricrin and K10 were reduced (45). Thus, the relevance of K10 and loricrin as ligands for *S. aureus* in AD remains unclear. The possibility that CDSN serves as a ligand in the nasal cavity of AD patients to facilitate nasal colonization was not investigated here. However, it will be interesting to examine if CDSN is accessible to bacteria on the nasal squamous epithelium given the apparent high incidence of nasal colonization among the pediatric AD population (46).

We previously showed that the cell wall-anchored protein ClfB mediates adhesion of *S. aureus* to low-NMF corneocytes from AD patients (6). Here, we show that FnBPB also has a role in corneocyte adhesion in AD. Surprisingly, there was no further reduction in the binding of a double *clfB fnbB* mutant compared with the single mutants. The double mutant was unable to adhere to CDSN in vitro, suggesting that additional *S. aureus* adhesins recognize a different ligand on corneocytes. This observation fits well with the finding that blocking the N-terminal region of CDSN with an antibody did not completely inhibit the binding of *S. aureus* to the corneocyte surface. Nevertheless, the binding to CDSN is a governing interaction between *S. aureus* and low-NMF corneocytes. We conclude, based on our data, that other adhesins produced by *S. aureus* promote adhesion to the corneocyte. These adhesins do not recognize CDSN (Fig. 1) or loricrin (6), leading us to speculate that an additional ligand exists. Future studies will focus on identifying the full repertoire of adhesins and their ligands operating at the *S. aureus*–corneocyte interface during colonization.

Skin colonization in AD is a complex and multifaceted process, involving microbial and host components. To successful colonize skin, *S. aureus* must avoid competition and interference from other components of the skin microbiota, overcome host defenses, and acquire nutrients. This study defines a key interaction occurring at the *S. aureus*–corneocyte interface. We propose that ClfB and FnBPB mediate adherence to CDSN, facilitating adhesion to the stratum corneum and allowing *S. aureus* to establish its niche. We hypothesize that the ability of *S. aureus* to dominate the skin microbiome in moderate to severe AD could be a consequence of its particular capacity to bind AD corneocytes via ClfB and FnBPB. This insight broadens our understanding of the complex host–pathogen interaction that occurs during colonization.

Materials and Methods

Bacterial Strains and Plasmids. *S. aureus* strains were grown in tryptic soy broth (TSB) at 37 °C with shaking (200 rpm). *E. coli* strains were grown at 37 °C in lysogeny broth with shaking at 37 °C. Antibiotics were added to the media where appropriate: ampicillin (100 μg/mL), chloramphenicol (10 μg/mL), and anhydrotetracycline (1 μg/mL).

***S. aureus* Mutants and Complementation.** All strains and plasmids are listed in *SI Appendix*. *S. aureus* mutants were generated by allelic exchange using the plasmid pIMAY. Deletion of the *clfB* gene to generate AD08Δ*clfB* was performed as described by Fleury et al. (6). Deletion of the *fnbA* and *fnbB* genes in AD08 and AD08Δ*clfB* was achieved using plasmid pIMAY. Primers for cloning DNA into pIMAY contained 5′ extensions with homology to the vector and are listed in *SI Appendix*, Table S3. A linear pIMAY product was generate by carrying out PCR using pIMAY Inv F and pIMAY Inv R primers. To construct pIMAYΔ*fnbAfnbB*$_{CC1}$, a DNA fragment comprising 600 nucleotides upstream of *fnbA* was amplified by PCR with primers fnbkoCC1A and fnbkoCC1B, and 600 nucleotides downstream of *fnbB* were amplified with primers fnbkoCC1C or fnbkoCC1D using genomic DNA from MSSA476 as template. The upstream and downstream fragments were joined using splicing by overlap-extension PCR and cloned into linearized pIMAY using sequence- and ligation-independent cloning (47) to generate plasmid pIMAYΔ*fnbAfnbB*$_{CC1}$. Deletion of the *fnbA* gene in AD08 and AD08Δ*clfB* was achieved using plasmid pIMAY::Δ*fnbA* to produce AD08Δ*fnbA* and AD08Δ*clfB*Δ*fnbA*, respectively. To create pIMAY::Δ*fnbA*, regions 500 bp upstream and 504 bp downstream of the *fnbA* gene were amplified from AD08 genomic DNA using primers fnbA A, fnbA B, fnbA C, and fnbA D. The up- and downstream PCR products were denatured and allowed to reanneal via complementary sequences in primers fnbA B and fnbA C, which were used as template for subsequent PCR with primers fnbA A and fnbA D. The product was cloned into pIMAY between KpnI and SacI restriction sites using sequence- and ligation-independent cloning to generate plasmid pIMAY::Δ*fnbA*. AD08Δ*clfB* and AD08Δ*clfB*Δ*fnbA*Δ*fnbB* were constructed by deletion of the *clfB* gene in AD08 and AD08Δ*fnbA*Δ*fnbB*, respectively, using plasmid pIMAY::Δ*clfB*. The *fnbA* gene was restored to its original location on the chromosome of AD08Δ*fnbA*Δ*fnbB* and AD08Δ*clfB*Δ*fnbA*Δ*fnbB* using plasmid pIMAY::*fnbA*_restore to generate AD08Δ*fnbB* and AD08Δ*clfB*Δ*fnbB*, respectively. Plasmid pIMAY::*fnbAfnbB*$_{CC1}$ was used as template for an inverse PCR with primers fnbB_Del F and fnbB_Del R to delete the *fnbB* gene sequence. The product was joined by blunt-end ligation using LigaFast Rapid DNA Ligation System (Promega) to generate plasmid pIMAY::*fnbA*_restore. The sequences of DNA cloned in pIMAY were verified by DNA sequencing of the plasmids (GATC Biotech). Each plasmid was passaged through *E. coli* IM01B to allow for subsequent transformation of *S. aureus* AD08 as previously described (48). Following allelic exchange, mutations were confirmed by DNA sequencing of a PCR amplimer. The mutants were phenotypically identical to the AD08 parent strain in terms of growth rate and δ-toxin activity. Complementation was achieved with plasmid pALC2073:*fnbB* or pCU1:*clfB*. The *fnbB* gene was amplified with primers fnbB_F and FnbB R using AD08 genomic DNA as template, and the pALC2073 vector was linearized by amplifying with the primers pALC Inv F and pALC Inv R. The *fnbB* gene was cloned between EcoRI and SacI restriction sites using sequence- and ligation-independent cloning to generate plasmid pALC2073:*fnbB*. Plasmids pALC2073:*fnbB* and pCU1:*clfB* were passaged through IM01B and transformed into AD08Δ*clfB*Δ*fnbB*.

CDSN Constructs. A DNA fragment encoding amino acid residues 33 to 529 of human CDSN codon optimized for *E. coli* (Integrated DNA Technologies) was amplified by PCR using primers incorporating BglII and SalI restriction sites,

cloned into the expression vector pGEX-4T2 (GE Lifesciences), and used to transform *E. coli* strain XL1-Blue. The recombinant plasmid was isolated from *E. coli* and used as template for inverse PCR using primers CDSN F ST and CDSN R ST to incorporate DNA encoding a Strep tag II affinity tag at the 3′ end of the *CDSN* gene generating plasmid pGEX-4T2::*CDSN*. Plasmids pGEX-4T2::*CDSNΔCT* and pGEX-4T2::*CDSNΔNT* were generated by inverse PCR using pGEX-4T2::*CDSN* as template and primers CDSNΔCT F, CDSNΔCT R and CDSNΔNT F, CDSNΔNT R, respectively. Plasmid pGEX-4T2::*CDSN*NTΩloop was constructed by two consecutive rounds of inverse PCR using pGEX-4T2::*CDSN* as template and primers $CDSN\Delta_{33–61}$ F, $CDSN\Delta_{33–61}$ R and $CDSN\Delta_{172–529}$ F, $CDSN\Delta_{172–529}$ R, respectively. Inverse PCR products were joined by blunt-end ligation and used to transform *E. coli* XL-1 Blue. Plasmids were isolated from XL-1 Blue and used to transform *E. coli* expression strain Topp3.

Recombinant Protein Expression and Purification. Cultures of *E. coli* Topp3 carrying expression vectors were grown to an optical density at 600 nM (OD_{600}) of 0.6 to 1. Protein expression was induced by isopropylß-D-1-thiogalactopyranoside (1 mM; VWR Chemicals) for 3 to 5 h, after which the bacteria were harvested and lysed using a French Pressure Cell at 1,500 psi. Recombinant GST-tagged CDSN proteins were purified by glutathione affinity chromatography followed by Strep-Tactin affinity chromatography and analyzed by sodium dodecyl sulphate-polyacrylamide gel electrophoresis. Recombinant GST-tagged recombinant human loricrin and human K10 peptide (19) were purified by glutathione affinity chromatography. Recombinant His-tagged $rClfB_{CC1}N2N3$ and $rFnBPB_{CC1}N2N3$ proteins were purified using nickel affinity chromatography as described previously (6). Protein concentrations were determined by measuring absorbance at 280 nm using a Nanodrop spectrophotometer according to Beer–Lambert Law or by BCA Protein Assay Kit (Pierce) as per the manufacturer's instructions.

Bacterial Adherence Assay. The wells of a microtiter plate (Nunc Maxisorb) were coated with rCDSN diluted in sodium carbonate butter (0.1 M $NaHCO_3$, pH 9.6) and incubated overnight at 4 °C. Coated wells were blocked with 5% (wt/vol) bovine serum albumin (Fisher) for 2 h at 37 °C. Bacterial cultures were grown to exponential phase (OD_{600} = 0.35) in TSB and adjusted to OD_{600} = 1.0 in phosphate buffered saline (PBS); 100 μL of bacterial suspension was added to each well, and the plate was incubated for 2 h at 37 °C. The plate was washed with PBS before adding formaldehyde (25% vol/vol; Sigma) to fix adherent cells. Fixed cells were stained with crystal violet (0.5% wt/vol), and absorbance was measured at 570 nm.

SPR. SPR was performed using a Biacore ×100 system (GE Healthcare). His-tagged human rCDSN (25 μg/mL; Source Bioscience UK Ltd) was diluted in 10 mM sodium acetate buffer at pH 4.0 and immobilized onto one flow cell of a CM5 sensor chip by amine coupling as described by the manufacturer. A second flow cell remained uncoated and served as a reference surface. Increasing concentrations of $rClfB_{CC1}N2N3$ (6) or $rFnBPB_{CC1}N2N3$ (also known as FnBPB N2N3 isotype III) (39) were passed over the surface of the chip. The surface of the chip was regenerated with 1 M NaCl between individual cycles. All sensorgram data were subtracted from the corresponding data from the reference flow cell. The response generated from passing buffer over the chip surface was also subtracted from each sensorgram. Data were analyzed using BIAevaluation software (3.0). The K_D for each interaction was calculated by plotting the level of binding (response units) against the concentration of $rClfB_{CC1}N2N3$ and $rFnBPB_{CC1}N2N3$.

Corneocyte Collection. Corneocytes were collected from a clinically unaffected site on the volar part of the patient's forearm using a tape stripping method described previously (49). Samples were deidentified prior to use in this study. Briefly, circular adhesive tape strips (3.8 cm^2; D-Squame, Monaderm) were attached to the target site on the patient's forearm, and pressure (225 g/cm^2) was applied for 10 s using a D-Squame pressure instrument (D500; CuDerm). The tape strip was transferred into a vial for storage at −80 °C. Eight consecutive tape strips were sampled from the same site. The fourth strip was used for NMF measurements, while the seventh or eighth consecutive strip was used to measure bacterial binding.

NMF Measurement. NMF analysis was performed on tape strips using a previously described method (50). Briefly, the tape strip was extracted using 25% (wt/wt) ammonia solution followed by evaporation of the ammonia extract. The residue was then dissolved in 500 μL of Millipore water and analyzed using high performance liquid chromatography. Due to variations in stratum corneum content on the tape strip, the NMF concentration was normalized for the protein amount determined by a Pierce Micro Bicinchoninic Acid Protein Assay Kit (Thermo Fisher Scientific).

Corneocyte Adherence Assay. A single tape strip was cut into quadrants, and each quadrant was placed into a different well of a six-well plate. Bacteria were grown to exponential phase (OD_{600} = 0.35) in TSB and adjusted to OD_{600} = 0.1 in 1 mL PBS; 100 μL of bacterial suspension was placed onto each tape strip quadrant and incubated for 1 h at 37 °C. Following incubation, 2 mL of PBS was added to each well, and quadrants were washed three times with 800 μL PBS. Cells were fixed using the cytological fixative CytofixxTM (Cellpath) and allowed to dry for 15 min. Quadrants were stained using crystal violet (0.0025%; wt/vol), washed in H_2O, and allowed to dry for 30 min. Quadrants were mounted onto glass slides, and coverslips (25 × 50 mm) were overlaid using the mountant D.P.× (BDH). Corneocytes were visualized under a microscope at 1,000× magnification, and the number of adherent bacteria per corneocyte was counted (single blind).

AFM.

Anti-CDSN antibody recognition.

AFM probe functionalization. MSCT probes (Bruker) were functionalized with polyclonal immunoglobulin G raised against $CDSN_{40–229}$ (anti-CDSN IgG; AntibodyGenie) as follows, based on the method of Wilding et al. (51). Prior to functionalization, cantilevers were thoroughly cleaned in chloroform and ethanol, dried with $N_{2(g)}$, and placed in an ultraviolet-ozone cleaner for 10 min. They were immersed in an ethanolamine solution (5 g ethanolamine, 10 mL dimethyl sulfoxide [DMSO]) overnight, rinsed in DMSO (3 × 1 min) and ethanol (3 × 1 min), and dried with $N_{2(g)}$. Ethanolamine-coated probes were then immersed for 2 h in a solution containing 1 mg of the acetal-polyethylene $glycol_{18}$-*N*-hydroxysuccinimide linker dissolved in 0.5 mL of chloroform and containing 30 μL of triethylamine, washed with chloroform, and dried with $N_{2(g)}$. Probes were further immersed in 1% citric acid for 10 min, washed in ultrapure water, and covered by a droplet of ∼100 μL of PBS solution with 0.1 mg/mL anti-CDSN antibody, to which 2 μL of $NaCNBH_3$ solution (1 M; with 20 mM NaOH) was added. After 1 h of incubation, 5 μL of ethanolamine (1 M; pH 8.0) was added to the drop on the cantilevers and left to incubate for 10 min. Probes were finally washed with buffer (3 × 5 min) and kept in buffer until used for AFM experiments.

Single-molecule force spectroscopy experiments. Using anti-CDSN functionalized AFM probes, we measured the interaction frequency and force between corneocytes coming from two patients, one presenting a wild-type filaggrin genotype and a high-NMF level and one presenting a heterozygous genotype and a low-NMF level (*SI Appendix*, Table S4). A piece of corneocyte-bearing tape strip was carefully cut out and immobilized on the bottom of a polystyrene petri dish with double-sided tape, corneocytes facing up, and the petri dish was filled with PBS buffer. For each corneocyte probed, we performed force volumes over 1- × 1-μm area of the corneocyte, with 32 × 32 force–distance curves acquired. The 1,024 curves obtained per experiment were then analyzed using the data processing software from JPK Instruments (now part of Bruker) to quantify the adhesion probability and force. Six independent experiments (i.e., independent AFM tip vs. corneocyte) were performed for low- and high-NMF skins. Each functionalized AFM probe was used to probe both low- and high-NMF corneocytes successively, with alternate orders for each new probe.

CDSN blocking.

Cell probe preparation. Colloid probes were prepared by gluing single silica microspheres (6.1-μm diameter; Bangs Laboratories and ultraviolet curable glue NOA 63; Norland Edmund Optics) onto tipless NPO-10 cantilevers (Bruker), as described earlier (52) using a Nanowizard III AFM (JPK Instruments; now part of Bruker). After 1 h of incubation in a polydopamine solution (tris-buffered saline [50 mM Tris, 150 mM NaCl, pH 8.5] containing 4 mg/mL dopamine hydrochloride [Sigma-Aldrich]) and rinsing in tris-buffered saline, the probe was mounted on the AFM probe holder and used to immobilize a single bacterium on the colloidal probe. The nominal spring constant of the colloidal probe cantilever was of ∼0.06 N/m, as determined by the thermal noise method.

Single-cell force spectroscopy experiment. *S. aureus* AD08 was cultured overnight, harvested by centrifugation, washed twice in PBS, and diluted 1:10 in PBS. A 50-μL droplet of bacterial suspension was deposited at one extremity of a polystyrene petri dish, while low-NMF corneocytes were immobilized at a distinct location in the petri dish, using the procedure described by Formosa-Dague et al. (53). The petri dish was filled with 2 mL of PBS buffer, and a polydopamine-coated colloidal probe was brought in contact with an isolated bacterium and retracted to immobilize the bacterium, whose attachment was checked by optical microscopy. The cell probe was repositioned above the corneocyte sample while remaining in the experimental liquid volume. The bacterium–corneocyte interactions were

MICROBIOLOGY

measured at room temperature, with an applied force of 0.25 nN, a constant approach/retract speed of 1 μm/s, and a contact time of 0.1 s. $F(ab')_2$ fragments of polyclonal rabbit IgG raised against $CDSN_{40–229}$ (AntibodyGenie) were generated using the Pierce $F(ab')_2$ Micro Preparation Kit as per the manufacturer's instructions. The $F(ab')_2$ antibody fragment was injected into the experimental volume at increasing concentrations during the single-cell force spectroscopy experiment, in order to probe the evolution of the interaction of each bacterium–corneocyte pair as a function of $F(ab')_2$ concentration. Data were analyzed using JPK Instrument software, extracting the adhesion probability.

Western and Whole-Cell Immunoblotting. For western blots, purified recombinant GST-tagged proteins (1.38 μM) were incubated with human thrombin (100 U/mL) for 2 h at 25 °C, boiled for 10 min in Laemmli final sample buffer (Sigma), separated on polyacrylamide gels, and transferred onto polyvinylidene difluoride (Roche). Filters were blocked in 10% (wt/vol) skimmed milk proteins before being probed with anti-CDSN IgG (1:3,000) followed by goat anti-rabbit IgG-horseradish peroxidase (1:3,000; DAKO). For whole-cell immunoblots, AD08 was grown overnight in TSB, and bacteria were washed twice with PBS and resuspended to an OD_{600} = 4.0 in PBS. Doubling dilutions (5 μL) were spotted on a nitrocellulose filter (Protran). The filter was blocked in 10% (wt/vol) skimmed milk proteins for 1 h and probed with anti-CDSN $F(ab')_2$ fragments (0.05 μg/mL) or anti-ClfA polyclonal IgG (1:2,000) followed by goat anti-rabbit IgG-horseradish peroxidase (1:3,000; DAKO). Reactive bands were visualized using the LumiGLO reagent and peroxide detection system (Cell Signaling Technology).

Ethical Approval. The study was conducted in accordance with the Helsinki Declaration and was approved by the Research Ethics Committee of Our Lady's Children's Hospital, Crumlin, Dublin, Ireland.

Statistical Analysis. Statistical analyses were performed using GraphPad Prism and Origin pro software. A P value < 0.05 was considered significant.

Data Availability. All study data are included in the article and *SI Appendix*.

ACKNOWLEDGMENTS. This study was funded by a British Skin Foundation Research Project grant (to J.A.G.). We acknowledge the support of the National Children's Research Centre, Dublin for our clinical studies. T.M.D.C. is supported by an Irish Research Council Postdoctoral Fellowship. Work at Université Catholique de Louvain was supported by the European Research Council under the European Union's Horizon 2020 Research and Innovation Programme Grant 693630, the National Fund for Scientific Research (FNRS), and FNRS–Walloon Excellence in Life Sciences and Biotechnology (WELBIO) Grants WELBIO-CR-2015A-05 and WELBIO-CR-2019S-01. Y.F.D is a research director at the FNRS. We thank Marta Zapotoczna for assistance with plasmid construction, Tim Foster for helpful discussion, Deirdre Muldowney for technical assistance, and Martin Sutton and Mary Turley for assistance with immunoblotting.

1. T. Bieber, Atopic dermatitis. *Ann. Dermatol.* **22**, 125–137 (2010).
2. S. Weidinger, L. A. Beck, T. Bieber, K. Kabashima, A. D. Irvine, Atopic dermatitis. *Nat. Rev. Dis. Primers* **4**, 1 (2018).
3. K. Eyerich, S. Eyerich, T. Biedermann, The multi-modal immune pathogenesis of atopic eczema. *Trends Immunol.* **36**, 788–801 (2015).
4. T. Bieber, Atopic dermatitis. *N. Engl. J. Med.* **358**, 1483–1494 (2008).
5. J. E. Totté *et al*., Prevalence and odds of *Staphylococcus aureus* carriage in atopic dermatitis: A systematic review and meta-analysis. *Br. J. Dermatol.* **175**, 687–695 (2016).
6. O. M. Fleury *et al*., Clumping factor B promotes adherence of *Staphylococcus aureus* to corneocytes in atopic dermatitis. *Infect. Immun.* **85**, e00994-16 (2017).
7. M. Yeung *et al*., Identification of major clonal complexes and toxin producing strains among *Staphylococcus aureus* associated with atopic dermatitis. *Microbes Infect.* **13**, 189–197 (2011).
8. M. L. Clausen *et al*., *Staphylococcus aureus* colonization in atopic eczema and its association with filaggrin gene mutations. *Br. J. Dermatol.* **177**, 1394–1400 (2017).
9. C. P. Harkins *et al*., The microevolution and epidemiology of *Staphylococcus aureus* colonization during atopic eczema disease flare. *J. Invest. Dermatol.* **138**, 336–343 (2018).
10. M. Tauber *et al*., *Staphylococcus aureus* density on lesional and nonlesional skin is strongly associated with disease severity in atopic dermatitis. *J.Allergy Clin. Immunol.* **137**, 1272–1274.e3 (2016).
11. H. H. Kong *et al*.; NISC Comparative Sequence Program, Temporal shifts in the skin microbiome associated with disease flares and treatment in children with atopic dermatitis. *Genome Res.* **22**, 850–859 (2012).
12. Y. Nakamura *et al*., Staphylococcus δ-toxin induces allergic skin disease by activating mast cells. *Nature* **503**, 397–401 (2013).
13. T. M. Zollner *et al*., Colonization with superantigen-producing *Staphylococcus aureus* is associated with increased severity of atopic dermatitis. *Clin. Exp. Allergy* **30**, 994–1000 (2000).
14. H. Liu *et al*., *Staphylococcus aureus* epicutaneous exposure drives skin inflammation via IL-36-mediated T cell responses. *Cell Host Microbe* **22**, 653–666.e5 (2017).
15. S. Nakagawa *et al*., *Staphylococcus aureus* virulent PSMalpha peptides induce keratinocyte alarmin release to orchestrate IL-17-dependent skin inflammation. *Cell Host Microbe* **22**, 667–677 e5 (2017).
16. J. A. Geoghegan, A. D. Irvine, T. J. Foster, *Staphylococcus aureus* and atopic dermatitis: A complex and evolving relationship. *Trends Microbiol.* **26**, 484–497 (2018).
17. S. H. Cho, I. Strickland, M. Boguniewicz, D. Y. Leung, Fibronectin and fibrinogen contribute to the enhanced binding of *Staphylococcus aureus* to atopic skin. *J. Allergy Clin. Immunol.* **108**, 269–274 (2001).
18. C. Feuillie *et al*., Adhesion of *Staphylococcus aureus* to corneocytes from atopic dermatitis patients is controlled by natural moisturizing factor levels. *mBio* **9**, e01184-18 (2018).
19. M. E. Mulcahy *et al*., Nasal colonisation by *Staphylococcus aureus* depends upon clumping factor B binding to the squamous epithelial cell envelope protein loricrin. *PLoS Pathog.* **8**, e1003092 (2012).
20. E. J. Walsh, L. M. O'Brien, X. Liang, M. Hook, T. J. Foster, Clumping factor B, a fibrinogen-binding MSCRAMM (microbial surface components recognizing adhesive matrix molecules) adhesin of *Staphylococcus aureus*, also binds to the tail region of type I cytokeratin 10. *J. Biol. Chem.* **279**, 50691–50699 (2004).
21. L. M. O'Brien, E. J. Walsh, R. C. Massey, S. J. Peacock, T. J. Foster, *Staphylococcus aureus* clumping factor B (ClfB) promotes adherence to human type I cytokeratin 10: Implications for nasal colonization. *Cell. Microbiol.* **4**, 759–770 (2002).
22. M. D. Howell *et al*., Cytokine modulation of atopic dermatitis filaggrin skin expression. *J. Allergy Clin. Immunol.* **120**, 150–155 (2007).
23. C. Cornelissen *et al*., IL-31 regulates differentiation and filaggrin expression in human organotypic skin models. *J. Allergy Clin. Immunol.* **129**, 426–433.e8, (2012).
24. A. D. Irvine, W. H. McLean, D. Y. Leung, Filaggrin mutations associated with skin and allergic diseases. *N. Engl. J. Med.* **365**, 1315–1327 (2011).
25. C. N. Palmer *et al*., Common loss-of-function variants of the epidermal barrier protein filaggrin are a major predisposing factor for atopic dermatitis. *Nat. Genet.* **38**, 441–446 (2006).
26. A. V. Rawlings, C. R. Harding, Moisturization and skin barrier function. *Dermatol. Ther.* **17**, 43–48 (2004).
27. C. Riethmuller *et al*., Filaggrin breakdown products determine corneocyte conformation in patients with atopic dermatitis. *J. Allergy Clini. Immunol.* **136**, 1573–1580.e2 (2015).
28. C. Caubet *et al*., Homo-oligomerization of human corneodesmosin is mediated by its N-terminal glycine loop domain. *J. Invest. Dermatol.* **122**, 747–754 (2004).
29. T. J. Foster, J. A. Geoghegan, V. K. Ganesh, M. Höök, Adhesion, invasion and evasion: The many functions of the surface proteins of *Staphylococcus aureus*. *Nat. Rev. Microbiol.* **12**, 49–62 (2014).
30. M. Grundmeier *et al*., Truncation of fibronectin-binding proteins in *Staphylococcus aureus* strain Newman leads to deficient adherence and host cell invasion due to loss of the cell wall anchor function. *Infect. Immun.* **72**, 7155–7163 (2004).
31. M. Guerrin *et al*., Expression cloning of human corneodesmosin proves its identity with the product of the S gene and allows improved characterization of its processing during keratinocyte differentiation. *J. Biol. Chem.* **273**, 22640–22647 (1998).
32. S. Igawa *et al*., Aberrant distribution patterns of corneodesmosomal components of tape-stripped corneocytes in atopic dermatitis and related skin conditions (ichthyosis vulgaris, Netherton syndrome and peeling skin syndrome type B). *J. Dermatol. Sci.* **72**, 54–60 (2013).
33. S. Igawa *et al*., Incomplete KLK7 secretion and upregulated LEKTI expression underlie hyperkeratotic stratum corneum in atopic dermatitis. *J. Invest. Dermatol.* **137**, 449–456 (2017).
34. G. Pietrocola *et al*., Fibronectin-binding protein B (FnBPB) from *Staphylococcus aureus* protects against the antimicrobial activity of histones. *J. Biol. Chem.* **294**, 3588–3602 (2019).
35. G. Pietrocola *et al*., Molecular interactions of human plasminogen with fibronectin-binding protein B (FnBPB), a fibrinogen/fibronectin-binding protein from *Staphylococcus aureus*. *J. Biol. Chem.* **291**, 18148–18162 (2016).
36. F. M. Keane *et al*., Fibrinogen and elastin bind to the same region within the A domain of fibronectin binding protein A, an MSCRAMM of *Staphylococcus aureus*. *Mol. Microbiol.* **63**, 711–723 (2007).
37. E. J. Walsh, H. Miajlovic, O. V. Gorkun, T. J. Foster, Identification of the *Staphylococcus aureus* MSCRAMM clumping factor B (ClfB) binding site in the alphaC-domain of human fibrinogen. *Microbiology (Reading)* **154**, 550–558 (2008).
38. A. J. McCarthy, J. A. Lindsay, Genetic variation in *Staphylococcus aureus* surface and immune evasion genes is lineage associated: Implications for vaccine design and host-pathogen interactions. *BMC Microbiol.* **10**, 173 (2010).
39. F. M. Burke, N. McCormack, S. Rindi, P. Speziale, T. J. Foster, Fibronectin-binding protein B variation in *Staphylococcus aureus*. *BMC Microbiol.* **10**, 160 (2010).
40. D. Hohl *et al*., Characterization of human loricrin. Structure and function of a new class of epidermal cell envelope proteins. *J. Biol. Chem.* **266**, 6626–6636 (1991).
41. E. Candi, R. Schmidt, G. Melino, The cornified envelope: A model of cell death in the skin. *Nat. Rev. Mol. Cell Biol.* **6**, 328–340 (2005).

42. B. E. Kim, D. Y. Leung, M. Boguniewicz, M. D. Howell, Loricrin and involucrin expression is down-regulated by Th2 cytokines through STAT-6. *Clin. Immunol.* **126**, 332–337 (2008).
43. L. Bao *et al*., A molecular mechanism for IL-4 suppression of loricrin transcription in epidermal keratinocytes: Implication for atopic dermatitis pathogenesis. *Innate Immun.* **23**, 641–647 (2017).
44. A. Totsuka, M. Omori-Miyake, M. Kawashima, J. Yagi, Y. Tsunemi, Expression of keratin 1, keratin 10, desmoglein 1 and desmocollin 1 in the epidermis: Possible downregulation by interleukin-4 and interleukin-13 in atopic dermatitis. *Eur. J. Dermatol.* **27**, 247–253 (2017).
45. V. Pendaries *et al*., Knockdown of filaggrin in a three-dimensional reconstructed human epidermis impairs keratinocyte differentiation. *J. Invest. Dermatol.* **134**, 2938–2946 (2014).
46. A. Lebon *et al*., Role of *Staphylococcus aureus* nasal colonization in atopic dermatitis in infants: The generation R study. *Arch. Pediatr. Adolesc. Med.* **163**, 745–749 (2009).
47. M. Z. Li, S. J. Elledge, SLIC: A method for sequence- and ligation-independent cloning. *Methods Mol. Biol.* **852**, 51–59 (2012).
48. J. Löfblom, N. Kronqvist, M. Uhlén, S. Ståhl, H. Wernérus, Optimization of electroporation-mediated transformation: *Staphylococcus carnosus* as model organism. *J. Appl. Microbiol.* **102**, 736–747 (2007).
49. S. Kezic *et al*., Filaggrin loss-of-function mutations are associated with enhanced expression of IL-1 cytokines in the stratum corneum of patients with atopic dermatitis and in a murine model of filaggrin deficiency. *J. Allergy Clin. Immunol.* **129**, 1031–1039.e1 (2012).
50. I. Dapic, I. Jakasa, N. L. H. Yau, S. Kezic, A. Kammeyer, Evaluation of an HPLC method for the determination of natural moisturizing factors in the human stratum corneum. *Anal. Lett.* **46**, 2133–2144 (2013).
51. L. Wildling *et al*., Linking of sensor molecules with amino groups to amino-functionalized AFM tips. *Bioconjug. Chem.* **22**, 1239–1248 (2011).
52. A. Beaussart *et al*., Quantifying the forces guiding microbial cell adhesion using single-cell force spectroscopy. *Nat. Protoc.* **9**, 1049–1055 (2013).
53. C. Formosa-Dague *et al*., Forces between *Staphylococcus aureus* and human skin. *Nanoscale Horiz.* **1**, 298–303 (2016).